Theoretical formulation and experimental validation of brightness evaluation using digital cameras

Nobuaki Shimoji [a,*], Musashi Okizaki [b]

[a] Department of Engineering, Faculty of Engineering, University of the Ryukyus, 1 Senbaru, Nishihara, Okinawa 903-0213, Japan
[b] Program of Electrical and Systems Engineering, Faculty of Engineering, University of the Ryukyus, 1 Senbaru, Nishihara, Okinawa 903-0213, Japan

ARTICLE INFO

ABSTRACT

In this study, we formulated the brightness relation of two digital photos captured by a single digital camera and verified it experimentally. The experimental results suggested that the used zoom lens has an intrinsic error, thereby making accurate photometry difficult. However, by dividing the brightness by the intrinsic error of the zoom lens, performing accurate photometry is possible. The photometry results with the single camera suggested that the brightness relation derived, and the magnitude system in astronomical photometry are applicable to widespread general photometry.

1. Introduction

Photometry using digital media such as still/movie cameras is useful in many research fields. For example, in sky photometry, skyglow in night has been evaluated (Hönel et al., 2018; Jechow et al., 2018; Jechow et al., 2020; Kolláth et al., 2020); in aurora science, the brightness of aurora have been studied (Syrjäsuo and Donovan, 2004). The discharge such as sprites and elves in the upper atmosphere emit light. Plasma generated in laboratory experiment also emit light. It is widely known that in astronomy, the light of stars have been studied. These light radiated from the objects have inner information and these are essential in these research fields.

In the field of lightning research, studies have been conducted to observe the relation between channel current and brightness (Flowers, 1943; Idone and Orville, 1985; Gomes and Cooray, 1998; Wang et al., 2005; Amarasinghe et al., 2007; Zhou et al., 2013). However, there have been few studies focusing on the brightness of the lightning channel. So far, we have reported on the lightning photometry applying color science and astronomical photometry (Shimoji et al., 2016; Shimoji et al., 2017; Shimoji and Uehara, 2017; Shimoji and Nakano, 2019). The results reported in these studies have been obtained by analyzing the brightness of lightning channels shown in a digital photo captured by a digital camera, and defining the reference brightness as the maximum pixel value 255 in 256 (8-bit) levels, as there are no reference light sources such as Alpha Lyra (Vega) in astronomical photometry.

When the brightness of objects shown in some digital photos captured by both a single camera and/or different cameras are compared, the correction of brightness of the photo by the *F*-number, ISO gain, and exposure time for the use of a single camera needs to be considered, as well as pixel properties, (pixel area, in-pixel gain, and floating diffusion capacitance) for the use of different cameras needs to be added. If precise correction is realized, photometry using digital camera will be possible. In this study, we theoretically derived the brightness relation of two photos captured by a single camera and/or different cameras. The objective of this study is to confirm the brightness relation above for a single camera, by experiment. As verifying the brightness relation for different cameras needs advanced skills and environment (i.e., it is beyond the scope of this study), it will be considered in future work.

As stated in Ref. Shimoji et al. (2017), quantitative evaluation of the brightness will be possible on the basis of the human naked eye via the magnitude system in astronomical photometry. The magnitude system in astronomical photometry can be widely applied not only in lightning research. Therefore, we add the brightness evaluation using the magnitude system.

To verify whether the image sensor in the camera used is working properly, the image sensor properties (linearity, saturation, and pixel value for the ISO gain) were studied. The lens properties (pixel value for the focal length, and irradiance ratio for the *F*-number difference) were also studied. Then, photometry with a single camera was performed, and the brightness relation derived theoretically herein was verified.

---

2. Theoretical background

2.1. Lens property

It is well known that the irradiance E_e in watts per square meter (W · m^{-2}) on the image plane varies depending on the F-number of the camera zoom lens (for example, see Ref. Hecht (2002) Chapter 5). The F-number denoted by $F/\#$, which is dimensionless, is the ratio of the focal length f of the lens to the diameter D of the entrance pupil (hereinafter called effective aperture), that is, $F/\# = f/D$. The area of the effective aperture denoted S_{ap} is proportional to the square of its diameter D, i.e. $S_{ap} \propto D^2$. The image area on the image plane is proportional to the square of the focal length f. Thus, the irradiance E_e at the image plane is proportional to $(D/f)^2$, i.e. $E_e \propto (D/f)^2$. This can also be written as follows: $E_e \propto (F/\#)^{-2}$. This indicates that the irradiance E_e on the image plane can be adjusted by the F-number of the lens.

In general, the F-number $F/\#$ is shown as the sequence: $F/1, F/1.4, F/2, F/2.8, F/4, F/5.6, F/8, F/11, F/16$, and so on. The sequence above can be considered as the geometric sequence a_n with common ratio $r = 1/\sqrt{2}$,

$$a_1 = a, \ a_2 = ar, \ a_3 = ar^2, \ \dots, \ a_n = ar^{n-1}, \ \dots \quad (1)$$

that is, $a_1 = a = F/1 = F/(\sqrt{2})^0, a_2 = F/1.4 = F/(\sqrt{2})^1, a_3 = F/2 = F/(\sqrt{2})^2, a_4 = F/2.8 = F/(\sqrt{2})^3, a_5 = F/4 = F/(\sqrt{2})^4, a_6 = F/5.6 = F/(\sqrt{2})^5, a_7 = F/8 = F/(\sqrt{2})^6, a_8 = F/11, F/(\sqrt{2})^7, a_9 = F/16, F/(\sqrt{2})^8$, and so on. In this section §2.1, the nth F-number is written as an nth term a_n in the geometric sequence, as the symbol $F/\#$ is considered to be a ratio, and there is a possibility of confusion for the interpretation. An nth F-number is $\sqrt{2}^k$ times greater than an $(n-k)$th F-number; Similarly, an nth F-number is $\sqrt{2}^k$ times smaller than an $(n+k)$th F-number, i.e. $a_n = (\sqrt{2})^k a_{n-k} = (\sqrt{2})^{-k} a_{n+k}$ (see Figs. 1(a) and 2(a)). The ratio between the $(n-k)$th and nth terms of the sequence is given by
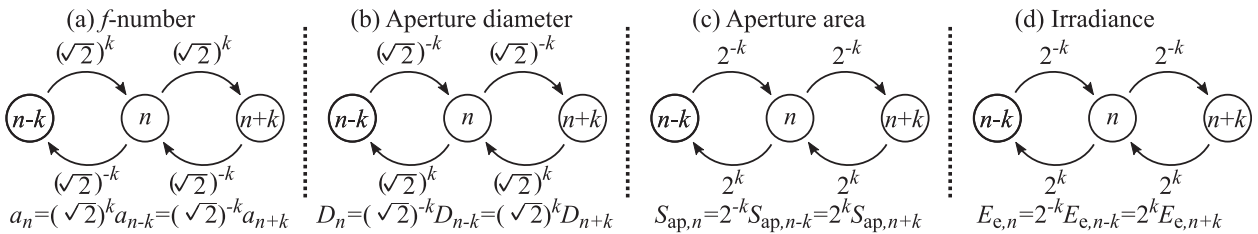
$$\frac{a_n}{a_{n-k}} = \frac{a_{n+k}}{a_n} = \left(\sqrt{2}\right)^k. \quad (2)$$

Taking the logarithm of both sides of Eq. (2) yields (see Fig. 3)

$$k = \log_{\sqrt{2}} \frac{a_n}{a_{n-k}} = \log_{\sqrt{2}} \frac{a_{n+k}}{a_n}, \quad (3)$$

where the base is the square root of 2. Thus, k indicates the difference between $(n-k)$th and nth F-number, or nth and $(n+k)$th F-number. The aperture diameter D_n of an nth F-number is $\sqrt{2}^k$ times smaller than D_{n-k} of an $(n-k)$th F-number as the nth F-number is $\sqrt{2}^k$ times higher than the $(n-k)$th F-number. The relation between the effective aperture diameters is given by

$$D_n = \left(\sqrt{2}\right)^{-k} D_{n-k} = \left(\sqrt{2}\right)^k D_{n+k}. \quad (4)$$

where D_{n-k}, D_n and D_{n+k} denote the aperture diameter of $(n-k)$th, nth, and $(n+k)$th F-number, respectively (see Figs. 1(b) and 2(b)). From the formula of the area of a circle having a diameter of D, i.e., $S = \pi(D/2)^2$, the area of the effective aperture of an nth F-number, $S_{ap,n}$ is given by

$$S_{ap,n} = 2^{-k} S_{ap,n-k} = 2^k S_{ap,n+k}, \quad (5)$$

where $S_{ap,n-k}$ and $S_{ap,n+k}$ denote the effective aperture area of the $(n-k)$th and $(n+k)$th F-number, respectively (see Figs. 1(c) and 2(c)). The irradiance E_e on an image plane is proportional to the aperture area, i.e. $E_e \propto S_{ap}^{-1}$. Eq. (5) indicates that the irradiance $E_{e,n}$ on the image plane, for an nth F-number is expressed by

$$E_{e,n} = 2^{-k} E_{e,n-k} = 2^k E_{e,n+k}, \quad (6)$$

where $E_{e,n-k}, E_{e,n}$, and $E_{e,n+k}$ denote the irradiance for the $(n-k)$th, nth, and $(n+k)$th F-number, respectively (see Figs. 1(d) and 2(d)).

2.2. CMOS image sensor

Fig. 4(a) shows a pixel array for a CMOS image sensor. Photons captured by a photodiode in a pixel array is converted to an electric

Fig. 1. Relations of (a) F-numbers, a_{n-k}, a_n, a_{n+k}, (b) aperture dimeter, D_{n-k}, D_n, D_{n+k}, (c) aperture area, $S_{ap,n-k}, S_{ap,n}, S_{ap,n+k}$, and (d) irradiance, $E_{e,n-k}, E_{e,n}, E_{e,n+k}$, for $(n-k)$th, nth, and $(n+k)$th F-numbers. The numbers $n-k, n$, and $n+k$ in the circles indicate the steps of the F-number.
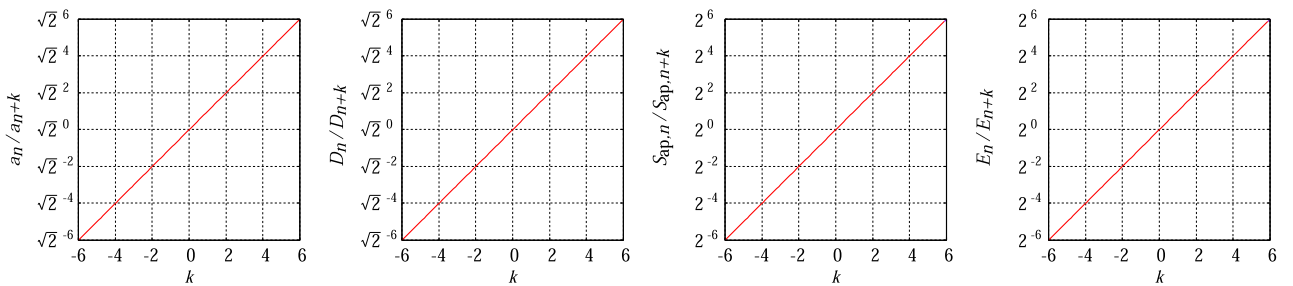

Fig. 2. (a) F-number ratio a_n/a_{n+k} vs. F-number difference k, (b) aperture diameter ratio D_n/D_{n+k} vs. k, (c) aperture area ratio $S_{ap,n}/S_{ap,n+k}$ vs k, and (d) irradiance ratio $E_{e,n}/E_{e,n+k}$ vs. k.
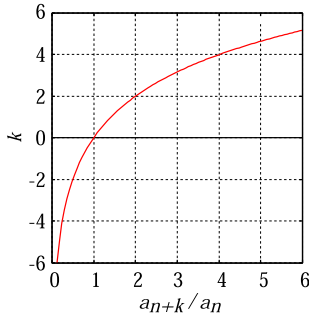
Fig. 3. *F*-number difference k vs. *F*-number ratio a_n/a_{n+k}.

voltage, and it is then amplified by the output amplifier with a gain G. In general, the digital value of RAW image data is converted from an analog signal (i.e. electric voltage above) using an analog-to-digital converter. A schematic in a pixel is shown in Fig. 4(b) (see Ref. Bigasa et al. (2006), Fossum and Hondongwa (2014)). Photons are converted to electrons by the pinned photodiode (PPD), and the electrons then transfer to the floating diffusion (FD) through the transistor gate (TG). The voltage V_{FD} of the FD is amplified by the source follower amplifier (SFA) having a gain β. The amplified signal goes to the column bus through the row select transistor (RS). The FD is reset by the transistor (Rst). Fig. 4(c) shows the illustration of conversion process from photons emitted from an object to an output voltage V. For simplicity, the transistors Rst and RS are not shown in Fig. 4(c). We assume that atmosphere, lens (optical system (OS)), on-chip-micro-lens (OCL), color filter (CF) have transmittance $\tau_{\text{air}}(\lambda)$, $\tau_{\text{OS}}(\lambda)$, $\tau_{\text{OCL}}(\lambda)$, and $\tau_{\text{CF}}(\lambda)$, respectively, and the PPD has a quantum efficiency $\eta_{\text{PPD}}(\lambda)$. Photons emitted from an object go through the atmosphere, to OS to OCL to CF and arrive at the PPD. Thus the electron number N_{e} generated by the PPD is expressed as

$$N_{\text{e}} = \int_{t_0}^{t_1} \int_{-\infty}^{\infty} \tau_{\text{air}} \, \tau_{\text{OS}} \, \tau_{\text{OCL}} \, \tau_{\text{CF}} \, \eta_{\text{PPD}} \, N_{\text{p}}(t, \lambda) \, d\lambda \, dt, \tag{7}$$

where t_0 and t_1 are the times of the beginning and end of exposure, and N_{p} is the number of photons from an object. Fig. 4(d) shows the simple schematic from the PPD in a pixel to the output voltage V. The output voltage V is given by

$$V = GV_{\text{SF}} = G\beta V_{\text{FD}} = G\beta \frac{Q}{C_{\text{FD}}} \tag{8}$$

$$= G\beta \frac{\text{e}^-}{C_{\text{FD}}} N_{\text{e}}, \tag{9}$$

where V_{SF} is the output voltage of the SFA, V_{FD} is the voltage of the FD, Q is the charge transferred from the PPD, and C_{FD} is FD capacitance in femtofarad (fF) (for C_{FD}, see, e.g., Ref. Kusuhara et al. (2016)). From Eq. (9), the electron number N_{e} generated by the PPD is given as

$$N_{\text{e}} = \frac{C_{\text{FD}}}{G\beta\text{e}^-} V. \tag{10}$$

2.3. Photometry

Fig. 5 illustrates camera photometry. The brightness of a digital photo can be adjusted by changing the *F*-number $F/\#$, ISO gain G, and exposure time t_{exp}. If the cameras "Camera I" and "Camera II" are different products, the pixel properties, pixel area S (μm^2), in-pixel gain β, and FD capacitance C_{FD} (fF) should also be considered.

From Eq. (10), for the light with energy $E = h\nu$ in joules (J), the irradiance $E_{\text{e},\nu}$ in $\text{W} \cdot \text{m}^{-2}$ of the PPD in the image sensor is given by

$$E_{\text{e},\nu} = h\nu \frac{N_{\text{e}}}{tS} = h\nu \frac{C_{\text{FD}}}{Gt\beta S\text{e}^-} V. \tag{11}$$

As the radiant flux of "Light Source" is r times greater than "Reference Source" (see Fig. 5), and Eq. (6), the irradiance relation between "Camera I" and "Camera II" can be written as

$$2^k E_{\text{e},\nu,\text{II}} = r E_{\text{e},\nu,\text{I}}, \tag{12}$$

where $E_{\text{e},\nu,\text{I}}$ and $E_{\text{e},\nu,\text{II}}$ are the irradiance for "Camera I" and "Camera II", respectively. Substituting Eq. (11) for Eq. (12),

$$2^k h\nu \frac{C_{\text{FD,II}}}{G_{\text{II}} t_{\text{II}} \beta_{\text{II}} S_{\text{II}} \text{e}^-} V_{\text{II}} = r h\nu \frac{C_{\text{FD,I}}}{G_{\text{I}} t_{\text{I}} \beta_{\text{I}} S_{\text{I}} \text{e}^-} V_{\text{I}}, \tag{13}$$

and thus,

$$rV_{\text{I}} = V_{\text{II}} 2^k \frac{G_{\text{I}}}{G_{\text{II}}} \frac{t_{\text{I}}}{t_{\text{II}}} \frac{\beta_{\text{I}}}{\beta_{\text{II}}} \frac{S_{\text{I}}}{S_{\text{II}}} \frac{C_{\text{FD,II}}}{C_{\text{FD,I}}}, \tag{14}$$

$$= V_{\text{II}} 2^k \frac{G_{\text{ref}}}{G_{\text{II}}} \frac{t_{\text{ref}}}{t_{\text{II}}} \frac{\beta_{\text{ref}}}{\beta_{\text{II}}} \frac{S_{\text{ref}}}{S_{\text{II}}} \frac{C_{\text{FD,II}}}{C_{\text{FD,ref}}}. \tag{15}$$

Eq. (15) indicates the brightness of the object ("Light Source") in "Photo II" captured by "Camera II" to the reference brightness of "Reference Photo" captured by "Camera I". The brightness rV_{I} to the reference is denoted by V_{I}', and we refer to the brightness V as a pixel value, although V is output voltage in V of a pixel in the image sensor.

2.4. Error

In fact, the pixel values V_{I}' and V_{II} have the error of the image sensor, δ_{I} and δ_{II}, respectively, and the zoom lens has the intrinsic error δ_{Lens}. Eq. (15) can be rewritten as

$$V_{\text{I}}'(1 + \delta_{\text{I}}) = rV_{\text{I}}(1 + \delta_{\text{I}}) \tag{16}$$

$$= V_{\text{II}}(1 + \delta_{\text{II}}) 2^k (1 + \delta_{\text{Lens}}) \times \frac{G_{\text{ref}}}{G_{\text{II}}} \frac{t_{\text{ref}}}{t_{\text{II}}} \frac{\beta_{\text{ref}}}{\beta_{\text{II}}} \frac{S_{\text{ref}}}{S_{\text{II}}} \frac{C_{\text{FD,II}}}{C_{\text{FD,ref}}}, \tag{17}$$
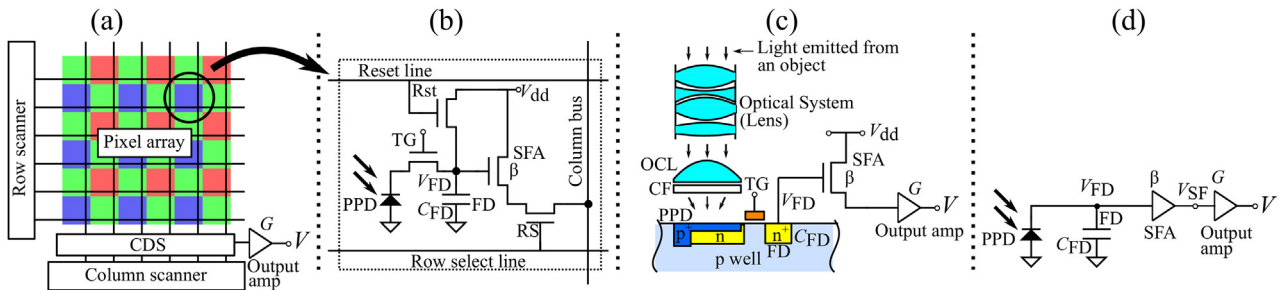
and thus,

Fig. 4. (a) Illustration of a CMOS image sensor. The CMOS image sensor scans an image generated by an optical system. The on-chip color filter array is a bayer pattern. (b) Schematic of a four transistor (4T) pixel. In a pixel, there are the PPD, FD, TG, Rst, SFA, and RS. (c) Illustration of conversion from photon emittted from an object to signal. In general, the PPD is embeded as shown. (d) Simple illustration from the PPD to the output.
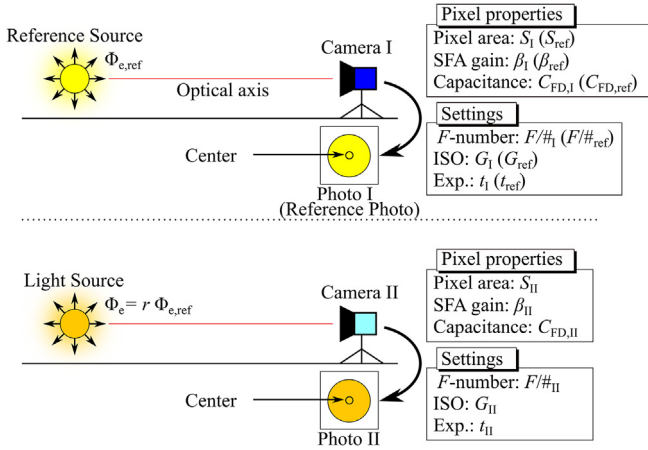
Fig. 5. Illustration of camera photometry. Suppose the light sources "Reference Source" and "Light Source" emits light equally in all directions, and these radiant fluxes in watts (W) are denoted by $\Phi_{e,ref}$ and $\Phi_e = r\Phi_{e,ref}$, respectively. "Camera I" has the following camera properties: pixel area S_I, source follower amplifier gain β_I, and FD capacitance $C_{FD,I}$, and "Camera II" has the camera properties: S_{II}, β_{II}, and $C_{FD,II}$. "Reference Source" is captured by "Camera I" with settings: F-number $F/\#_I$, ISO gain G_I, and exposure time t_I, and similarly "Light Source" is by "Camera II" with settings: $F/\#_{II}, G_{II}$, and t_{II}. The photos "Photo I" showing "Reference Source" and "Photo II" showing "Light Source" are generated by "Camera I" and "Camera II", respectively. When "Photo I" is assumed as the reference ("Reference Photo"), the camera settings and pixel properties of "Camera I" can be written as $F/\#_{ref}, G_{ref}, t_{ref}, \beta_{ref}, S_{ref}$, and $C_{FD,ref}$.

$$V'_I = rV_I = \quad V_{II} 2^k \frac{G_{ref}}{G_{II}} \frac{t_{ref}}{t_{II}} \frac{\beta_{ref}}{\beta_{II}} \frac{S_{ref}}{S_{II}} \frac{C_{FD,II}}{C_{FD,ref}} \times (1 + \delta_{Lens}) \frac{(1+\delta_{II})}{(1+\delta_I)}, (18)$$

$$\simeq V_{II} 2^k \frac{G_{ref}}{G_{II}} \frac{t_{ref}}{t_{II}} \frac{\beta_{ref}}{\beta_{II}} \frac{S_{ref}}{S_{II}} \frac{C_{FD,II}}{C_{FD,ref}} \times (1 + \delta_{Lens})(1 + \delta_{Sensor}), \quad (19)$$

since

$$
\begin{aligned}
(1 + \delta_{Lens}) \frac{(1+\delta_{II})}{(1+\delta_I)} &\simeq (1 + \delta_{Lens})(1 - \delta_I)(1 + \delta_{II}), \\
&\simeq (1 + \delta_{Lens})(1 - \delta_I + \delta_{II}), \quad (20)\\
&= (1 + \delta_{Lens})(1 + \delta_{Sensor}),
\end{aligned}
$$

where $(1 + \delta_I)^{-1} \simeq 1 - \delta_I$, $\delta_I \delta_{II} \simeq 0$, and the error of the image sensor is $\delta_{Sensor} = -\delta_I + \delta_{II}$. Eq. (19) shows that dividing V'_I by $(1 + \delta_{Lens})$ can reduce the intrinsic error of the zoom lens; similarly, dividing V'_I by $(1 + \delta_{Sensor})$ can reduce the error of the image sensor. As the intrinsic error δ_{Lens} is not a random error, it can be obtained in advance.

2.5. Magnitude of brightness

As explained in Ref. Shimoji et al. (2017) §1, the brightness to the reference can be expressed by magnitude system developed in astronomical photometry. By using Eq. (15), the magnitude of "Light Source" to "Reference Source" is given by

$$m = -2.5\log_{10} \frac{V'_I}{V_{ref}}, \quad (21)$$

$$= -2.5\log_{10} \frac{V_{II}}{V_{ref}} - 2.5\log_{10} 2^k \frac{G_{ref}}{G_{II}} \frac{t_{ref}}{t_{II}} \frac{\beta_{ref}}{\beta_{II}} \frac{S_{ref}}{S_{II}} \frac{C_{FD,II}}{C_{FD,ref}}, \quad (22)$$

where V_{ref} denotes the pixel value (reference brightness) of "Reference Source" in "Reference Photo" captured by "Camera I" (see Fig. 5). The second term of Eq. (22) is the correction term. In fact, Eq. (19) shows the magnitude containing the error of the zoom lens and the image sensor as follows

$$m = -2.5\log_{10} \frac{V'_I}{V_{ref}}, \quad (23)$$

$$
\begin{aligned}
= &-2.5\log_{10} \frac{V_{II}}{V_{ref}} - 2.5\log_{10} 2^k \frac{G_{ref}}{G_{II}} \frac{t_{ref}}{t_{II}} \frac{\beta_{ref}}{\beta_{II}} \frac{S_{ref}}{S_{II}} \frac{C_{FD,II}}{C_{FD,ref}} \\
&-2.5\log_{10}(1 + \delta_{Lens})(1 + \delta_{Sensor}).
\end{aligned}
\quad (24)
$$

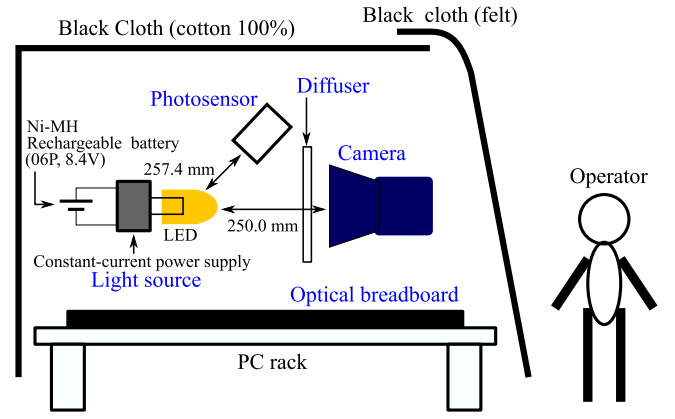**Fig. 6.** Schematic of the photography in the tabletop darkroom.

3. Materials and methods

3.1. Photography setup

Photography was performed in the tabletop darkroom (Fig. 6), which is explained in Appendix A. The digital camera (Nikon, D3200) with a zoom lens (Nikon, AF-SDX NIKKOR 18–55 mm f/3.5–5.6G VR) was located on the optical breadboard in the tabletop darkroom (see Fig. 6). We have developed a constant-current LED light source (Fig. 7 and a photosensor (Fig. 8). The design parameters of the tabletop darkroom, LED light source, and photosensor are shown in Table 1 (also see Appendix A). In this study, we chose R_1 (1 MΩ) as the feedback resistor R_f in the photosensor (Fig. 8), i.e., $V_P = 10^6 \times I_P$. The constant-current LED light source and photosensor were also located on the optical breadboard in the tabletop darkroom (see Fig. 6). The light emitted from the light source was monitored constantly during shooting, with the photosensor. The diffuser was located on the front of the zoom lens attached to the digital camera for enhancing light uniformity. At the time of the photography, the light outside the room was shielded by a blind, and the fluorescent light in the room was turned off.

3.2. Brightness at the center of the image plane

In this study, by evaluating the brightness on the image plane, we analyzed the pixel values of the 16 pixels on the 4 × 4 array at around the center of the CMOS image sensor (Fig. 9). This also reduces the influence of vignetting. We confirmed the pixels in the 4 × 4 array do not contain cool and hot pixels. Fig. 10 shows the flowchart of the averaging of the pixel values. The RAW data obtained from the camera should be converted to the PNM format image (more exactly, PGM image) at the (a) conversion process in Fig. 10, and the 4 × 4 array around the center of the PGM image was trimmed at the (b) trimming process in Fig. 10. Then, by (c) decomposition process in Fig. 10, the 4 × 4 PGM image trimmed was decomposed to B-channel having 4 pixels, G-channel having 8 pixels, and R-channel having 4 pixels. From the obtained B-channel, G-channel, and R-channel images, the average values of the pixels of these channels were obtained by calculating the following:

$$\overline{B}_{Pixel} = \frac{B_1 + B_2 + B_3 + B_4}{4}, \quad (25)$$

$$\overline{G}_{Pixel} = \frac{G_1 + G_2 + \cdots + G_8}{8}, \quad (26)$$

$$\overline{R}_{Pixel} = \frac{R_1 + R_2 + R_3 + R_4}{4}. \quad (27)$$

For noise reduction, the photography and processing (Fig. 10) were performed ten times, and the channel average values $\overline{B}, \overline{G}$, and $\overline{R}$ were calculated as follows (also see Fig. 11):
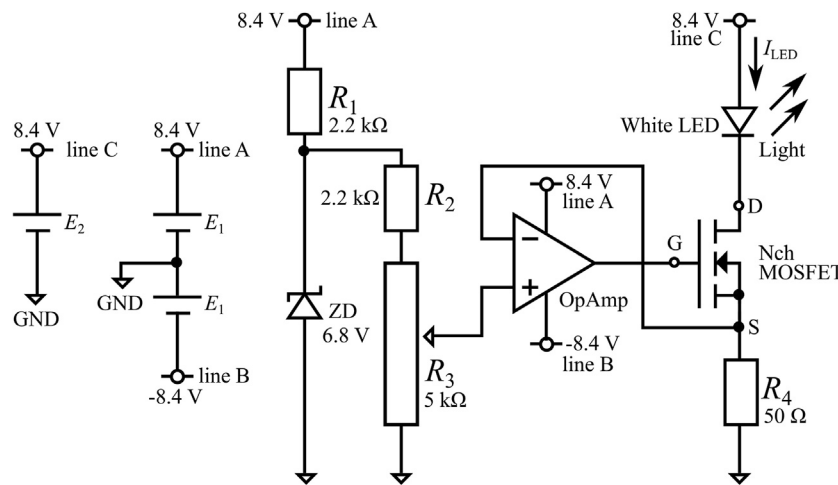
Fig. 7. Schematic of the constant-current driven white-LED light source. E_1 and E_2 are Ni-MH rechargeable batteries (for E_1, Toshiba, Impulse, 06P, for E_2, RS-PRO, 199–646, 06P), ZD is a zener-diode (Vishay, 1N5235B-TR), OpAmp is an operational amplifier (JRC, NJM072BD), Nch MOSFET is an N-ch MOSFET (Microchip, 2N7000-G), R_1 and R_2 are metal-film resistors, R_3 is a trimmer, R_4 (50 Ω) is composed of two resistors havig 100 Ω in parallel, and LED is a white-LED (Cree, C513A-WSN-CY0Z0231). The constant-current LED light source explained here was housed in a metal box. All signal grounds were connected to earth.
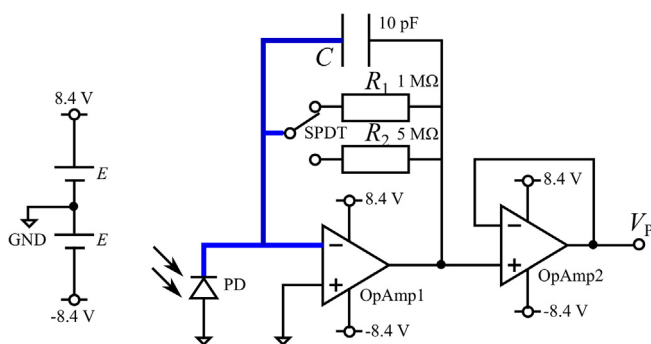

Fig. 8. Schematic of photosensor. E is a Ni-MH rechargeable battery (Toshiba, Impulse, 06P), PD is a photodiode (OSRAM Opto Semiconductors, SFH213), OpAmp1 and OpAmp2 are operational amplifiers (ANALOG DEVICES, OP07CPZ), SPDT is a single-pole dual-through switch, C is a seramic capacitor, R_1 and R_2 are metal film resistors. R_2 (5 MΩ) is composed of two resistors having 10 MΩ in parallel. The photodiode, non-inverting input of the OpAmp1, SPDT switch, and capacitor C were wired with a Teflon terminal (thick line). The photosensor explained here was housed in the metal box. All signal grounds were connected to earth.

$$\overline{B} = \frac{\overline{B}_{\text{Pixel,1}} + \overline{B}_{\text{Pixel,2}} + \overline{B}_{\text{Pixel,3}}}{3}, \qquad (28)$$

$$\overline{G} = \frac{\overline{G}_{\text{Pixel,1}} + \overline{G}_{\text{Pixel,2}} + \overline{G}_{\text{Pixel,3}}}{3}, \qquad (29)$$

$$\overline{R} = \frac{\overline{R}_{\text{Pixel,1}} + \overline{R}_{\text{Pixel,2}} + \overline{R}_{\text{Pixel,3}}}{3}. \qquad (30)$$

Herein, $\overline{B}, \overline{G}$, and $\overline{R}$ were evaluated as the pixel values (i.e., brightness) at the center of the image plane, i.e., $V_B = \overline{B}, V_G = \overline{G}$, and $V_R = \overline{R}$.

3.3. Image sensor properties

Before using the digital camera, it should be confirmed that the image sensor in the digital camera is working properly. We studied the image sensor properties: the linearity and saturation value of the image sensor, and the linearity for the ISO gain.

Table 1
Design parameters of the tabletop darkroom, constant-current LED light source, and photosensor.

Name	Design parameters
Tabletop darkroom	Size 60 W $\times$ 70D cm, Height of the tabletop 76 cm, Height of the shelf 124 cm
LED light source	Supply voltage ± 8.4 V, Maximum LED current $I_{\text{LED}} = 30$ mA, Typical luminous intensity $6,800$ mcd at $I_{\text{LED}} = 20$ mA and 25°C (regarding the luminous intensity, adapted from the datasheet of LED (Cree, C513A-WSN-CY0Z0231)).
Photosensor	Supply voltage ± 8.4 V, Output voltage range 0–7.7 V, The feedback resistor R_f can be switched between 1 MΩ and 5 MΩ. The output voltage V_P is given by $V_P = I_P R_f$, where I_P is the photocurrent generated by the photodiode.

3.3.1. Linearity and saturation value

The brightness of light emitted from the constant-current LED light source can be adjusted by the LED current I_{LED} (see Fig. 7). Changing the brightness of the constant-current LED light source, in the range $0 \leqslant I_{\text{LED}} \leqslant 20$ mA, we studied the change of the pixel values V_B, V_G, and V_R for B-, G-, and R-channels, at the center of the image sensor. The diffusers comprising one acrylic sheet (Fig. 12(a)) and three acrylic sheets (Fig. 12(b)) were used. The camera settings were as follows: focal length $f = 18$ mm, F-number $F/\# = 3.5$, ISO gain $G = 100$, exposure $t_{\exp} = 2$ s. Only in this experiment, the photography was performed three times for the noise reduction.

3.3.2. Linearity for the ISO gain

Though it is, in general, said that ISO gain is linear, we confirmed it. The diffuser comprising two acrylic sheets and four tracing papers (see Fig. 13) was used. The LED current of the LED light source (Fig. 7) was set to $I_{\text{LED}} = 20$ mA. The camera settings were as follows: focal length $f = 18$ mm, F-number $F/\# = 5.6, 11, 16$, and 22, ISO gain $G = 100, 200, 400, 800$, exposure $t_{\exp} = 1$ s. The pixel values V_B, V_G, and V_R vs. the ISO gain G were obtained.

3.4. Lens properties

The brightness of the digital photo captured by the digital camera are adjusted by the camera settings: focal length f, F-number $F/\#$, ISO
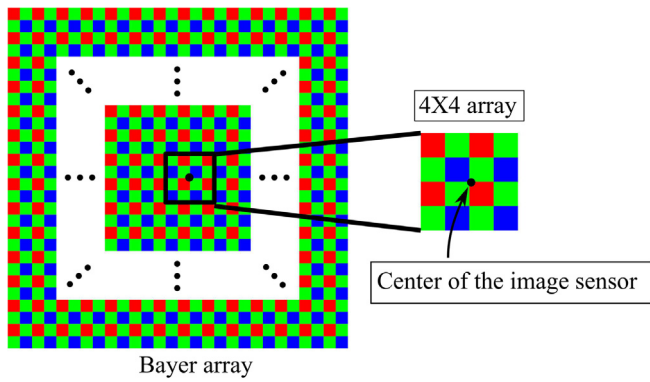
Fig. 9. Schematic of the 4×4 array around the center on the CMOS image sensor. Primary color filter of the digital camera used herein was a bayer filter, and the order of the bayer filter was RGGB. The solid circle is the center of the CMOS image sensor. The 16 pixels in the 4×4 array enclosed by the thick solid line were the evaluated pixels.

gain G, and exposure time t_{exp}, of which f and $F/\#$ are for lens. Thus, we have confirmed the relation between the pixel value V and the focal length f (V–f relation), and the relation between the irradiance ratio $E_{e,n}/E_{e,n+k}$ and the F-number difference k ($E_{e,n}/E_{e,n+k}$–k relation).

3.4.1. V–f relation

The diffuser shown in Fig. 13 was used. The LED current of the LED light source (Fig. 7) was set to $I_{\mathrm{LED}} = 20$ mA. We studied the change of the pixel values V_{B}, V_{G}, and V_{R} at the center of the image sensor, with respect to the change of the focal length f. The settings were as follows: F-number $F/\# = 5.6, 11, 16$, and 22, focal length $f = 18$ mm, 24 mm, 35 mm, 45 mm, 55 mm, ISO gain $G = 100$, and exposure time $t_{\mathrm{exp}} = 1$ s.

3.4.2. E_n/E_{n+k}–k relation

To check Eq. (6), we studied the irradiance ratio $E_{e,n}/E_{e,n+k}$ vs. the F-number difference k. The diffuser shown in Fig. 13 was used. The LED current of the LED light source (Fig. 7) was set to $I_{\mathrm{LED}} = 20$ mA. The camera settings except for the F-number were as follows: focal length
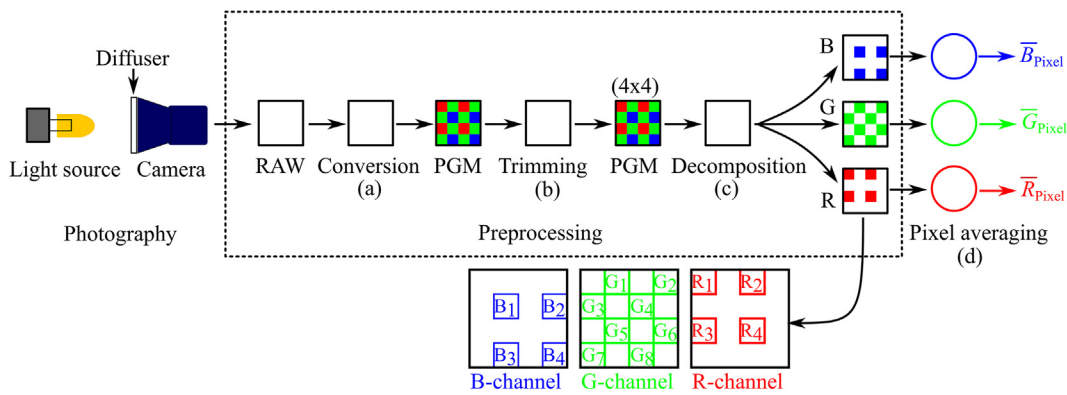

Fig. 10. Flowchart of pixel averaging. The preprocessing comprises three processing, (a) conversion from RAW data to a PGM image, (b) trimming which generates a 4×4 PGM image around the center of the image sensor, and (c) decomposition which generates 4×4 B-, G- and R-channel images. The 4×4 B-, G-, and R-channel images generated by (c) have four pixels (B_1, B_2, B_3, B_4) for B-channel, eight pixels ($G_1, G_2, ..., B_8$) for G-channel, and four pixels (R_1, R_2, R_3, R_4) for R-channel. The (d) pixel averaging generates three values $\overline{B}_{\mathrm{Pixel}}, \overline{G}_{\mathrm{Pixel}}$, and $\overline{R}_{\mathrm{Pixel}}$.
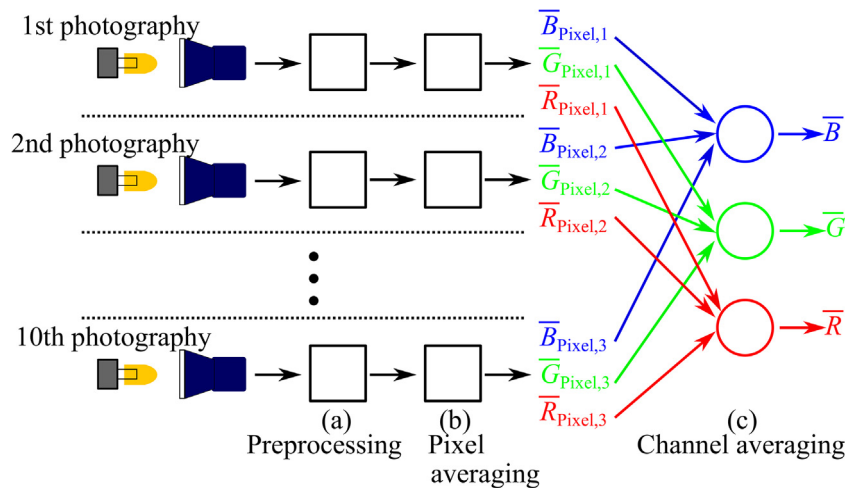

Fig. 11. Flowchart of averaging for noise reduction. The (a) preprocessing, (b) pixel averaging, and the pixel average values $\overline{B}_{\mathrm{Pixel}}, \overline{G}_{\mathrm{Pixel}}$, and $\overline{R}_{\mathrm{Pixel}}$ are explained in Fig. 10. The photography and processing (a) and (b) were done repeatedly ten times for noise reduction. The (c) channel averaging generates three average values $\overline{B}, \overline{G}$, and $\overline{R}$.
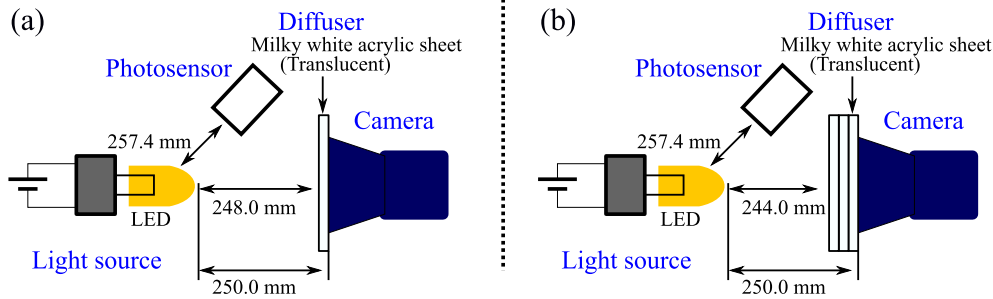
Fig. 12. Schematic of photography using the diffusers comprising (a) one acrylic sheet and (b) three acrylic sheets. The acrylic sheets (Kuraray, translucent milky white, matte on both sides, comoglass) have a size of 139.0 mm ×139.0 mm and a thickness of 2.0 mm.
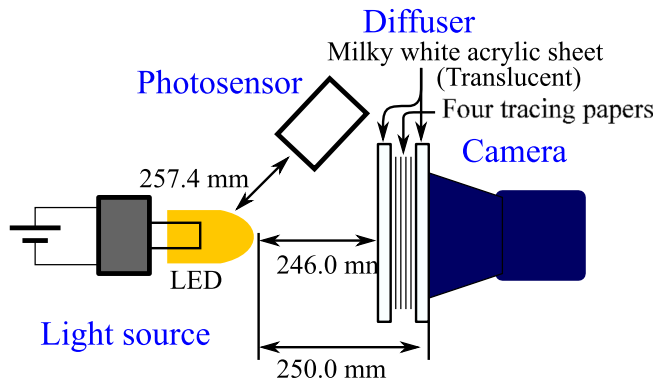

Fig. 13. Schematic of photography using the diffuser comprising two acrylic sheets (Kuraray, translucent milky white, matte on both sides, comoglass) with size 139.0 × 139.0 mm and thickness 2.0 mm, sandwitching four tracing papers (Sakae Technical Paper) with size 105.0 × 148.0 mm.

$f = 18\,\text{mm}, 35\,\text{mm}, 55\,\text{mm}$, ISO gain $G = 100$, exposure time $t_{\text{exp}} = 1$ s. The F-number for each focal length f is summarized in Table 2, as $F/\#$ and f are related to each other.

3.5. Photometry and magnitude with the single camera

The diffuser explained in Fig. 13 was used. For photography, we defined the reference settings as: focal length $f_{\text{ref}} = 18$ mm, F-number $F/\#_{\text{ref}} = 5.6$, ISO gain $G_{\text{ref}} = 100$, exposure time $t_{\text{ref}} = 1$ s. We also defined the reference brightness of the LED light source as the brightness at $I_{\text{LED}} = 20$ mA. Using Eq. (15) and Eq. (22), and based on the reference settings above, we studied V–k relation, V–ISO rela-

tion, and V–t_{exp} relation. The settings for the reference and the three relations are summarized in Table 3. In the photography, two brightness of the light source were adopted: one is the same as the reference brightness ($I_{\text{LED}} = 20$ mA), $\Phi_e = \Phi_{e,\text{ref}}$, i.e., $r = 1$, the other is half of the reference ($I_{\text{LED}} = 10$ mA), $\Phi_e = \Phi_{e,\text{ref}}/2$, i.e., $r = 1/2$ (also see §2.3 and Fig. 5).

4. Results and discussion

4.1. Linearity and saturation value

The output voltage V_{P} of the photosensor vs. the LED current I_{LED} in Fig. 14 show that the brightness change of the light emitted from the constant-current LED light source was linear. When the diffuser comprises one acrylic sheet (Fig. 12(a)), the pixel values V_{B}, V_{G}, and V_{R} (Fig. 14(a)) changed linearly, and these were saturated relatively quickly. The saturated values in $65,536$ (16-bit) levels were $\sim 65,000$ for B-channel, $\sim 62,000$ for G-channel, and $\sim 65,000$ for R-channel. For Fig. 14(b) using the three acrylic sheets (Fig. 12(b)), the pixel values V_{B} and V_{G} indicate linearity up to saturation values. We can see that V_{R} changed linearly, while the saturation for R-channel in Fig. 14(b) cannot be confirmed. Fig. 14 shows that the image sensor of the used camera works properly up to the saturation value $\sim 60,000$. Therefore, we defined the threshold value in $65,536$ (16-bit) levels of the saturation as $60,000$. In what follows, we focused only on the pixel values less than the saturation value of $60,000$.

4.2. Linearity for the ISO gain

Fig. 15 shows the pixel values V_{B}, V_{G}, and V_{R} for the ISO gain G. It is seen that the pixel value (brightness) V was increased linearly as

Table 2
F-numbers for the focal length $f = 18$ mm, 35 mm, and 55 mm.

Focal length																	*F*-number			
$f = 18$ mm	3.5	4	4.5	5	5.6	6.3	7.1	8	9	10	11	13	14	16	18	20	22	–	–	–	–
$f = 35$ mm	–	–	–	5	5.6	6.3	7.1	8	9	10	11	13	14	16	18	20	22	25	29	32	–
$f = 55$ mm	–	–	–	–	5.6	6.3	7.1	8	9	10	11	13	14	16	18	20	22	25	29	32	36

Table 3
Settings for the photography of the reference, and the V–k, V–ISO, and V–t_{exp} relation.

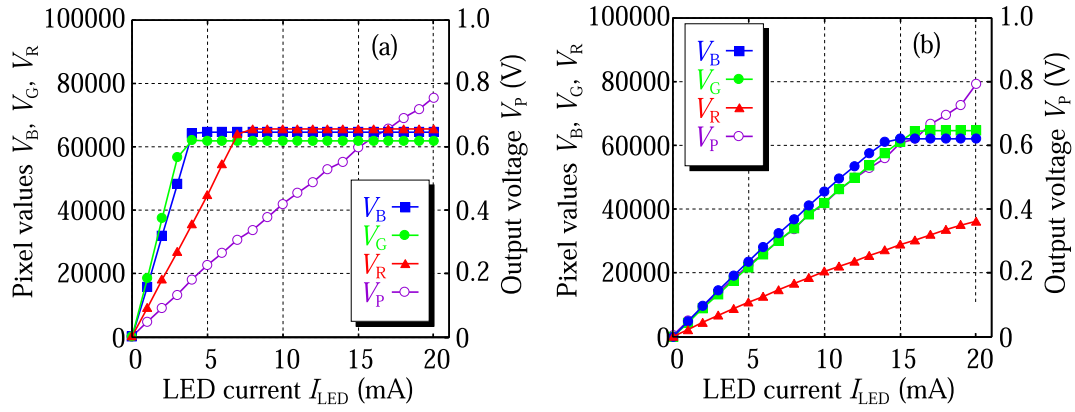|	f (mm)	F-number	ISO gain	Exposure time (s)
reference	18	5.6	100	1
V–k relation	18	$F/\#$ for $f = 18$ mm (see Table 2)	100	1
V–ISO relation	18	5.6	100, 200, 400, 800	1
V–t_{exp} relation	18	5.6	100	1/8, 1/4, 1/2, 1, 2, 4, 8

Fig. 14. Linearity of the CMOS image sensor and the brightness of the LED, for the diffusers comprising (a) one acrylic sheet and (b) three acrylic sheets. The B-, G-, and R-channel pixel values V_B, V_G, and V_R (left-side vertical axis) and output voltage V_P of the photosensor (right-side vertical axis) increases linearly with increasing LED current I_{LED}.
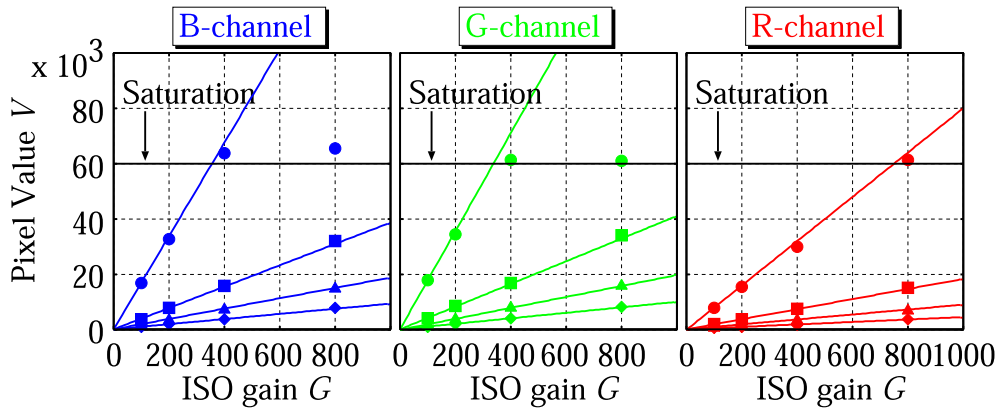

Fig. 15. Pixel value V vs. the ISO gain G for the B-, G-, and R-channels, and the F-number $F/\# = 5.6$ (solid circle), 11 (solid square), 16 (solid triangle), and 22 (solid diamond), with respect to the focal length $f = 18$ mm. The solid lines are obtained by $V_{ISO:100} \times G/G_{ISO:100}$.

Table 4
Mean relative error of V_B, V_G, and V_R with respect to the F-number $F/\# = 5.6, 11, 16$, and 22, and the focal length $f = 18$ mm.

F-number	Mean relative error %		
	Color		
	B	G	R
$F/\# = 5.6$	3.33	2.76	5.13
$F/\# = 11$	2.97	2.80	2.55
$F/\# = 16$	0.77	1.28	0.91
$F/\# = 22$	2.93	2.19	1.08

increasing the ISO gain G. The pixel value V at ISO:200, 400, and 800 are about 2, 4, and 8 times greater than that at the ISO:100, respectively. The mean relative errors of V_B, V_G, and V_R are summarized in Table 4; and the errors are less than ~5%. Thus, the brightness change for the ISO gain of the used camera is linear.

4.3. V–f relation

Fig. 16 shows the change of the pixel value for the focal length f, with the F-number $F/\# = 5.6, 11, 16$, and 22, ISO gain $G = 100$, exposure time $t_{exp} = 1$ s. In theory, if the F-number is constant, then the pixel value V is invariant, even if the focal length f changes. From Fig. 16, we found that there are variations in the data points. The vari-

ations of the pixel value are to be due to an intrinsic error of the zoom lens used herein. As the intrinsic error of the zoom lens is not a random error, it can be correct.

4.4. E_n/E_{n+k}–k relation

Fig. 17 shows the irradiance ratio $E_{e,n}/E_{e,n+k}$ vs. the F-number difference k with settings: focal length $f = 18$ mm, 35 mm, and 55 mm, ISO gain $G = 100$, and exposure time $t_{exp} = 1$ s. At first glance, the data points in Fig. 17 seems to fit to the theoretical curve 2^k, regardless of the difference between the B-, G-, and R-channels, and focal length $f = 18$ mm, 35 mm, and 55 mm, as the vertical axis is a logarithmic scale of base 2. However, the mean relative errors of these points are in the range of approximately 10%; and the maximum relative error is abnormally large at 34.34% at the settings $F/\# = 6.3, f = 18$ mm, $G = 100, t_{exp} = 1$ s in the B-channel (see Table 5). We have concluded that the deviation of the data points shown in Fig. 17 is due to the intrinsic error δ_{Lens} of the zoom lens used. (It is often said that commercially available zoom lens contain some errors.) The intrinsic error of the zoom lens will also be discussed in the next subsection §4.5 in more detail. When performing photometry using a digital camera with a zoom lens, investigating the intrinsic error from the theoretical curve 2^k in advance, for strict photometry is necessary. Within the tolerance, the relation $E_{e,n}/E_{e,n+k} = 2^k$ is applicable for photometry.
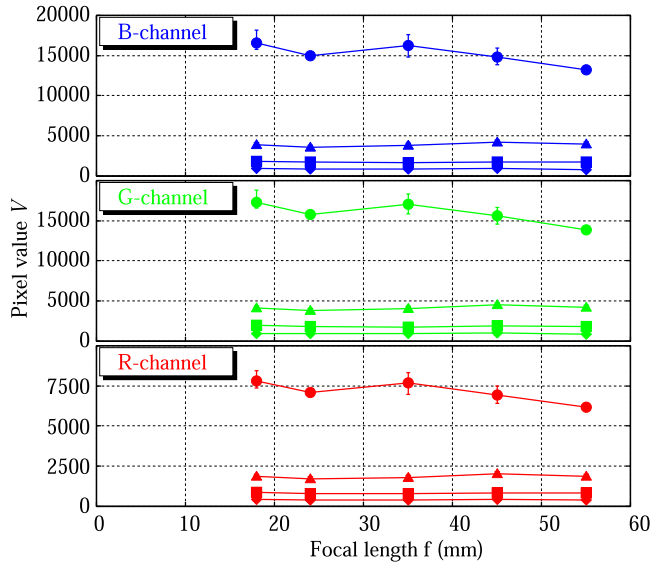
Fig. 16. Pixel value V vs. the focal length f for the B-, G-, and R-channels. The settings except for the focal length f were as follows: F-number $F/\# = 5.6$ (solid circle), 11 (solid triangle), 16 (solid square), and 22 (solid diamond), ISO gain $G = 100$, exposure time $t_{exp} = 1$ s.

4.5. Photometry and magnitude with the single camera

4.5.1. Reference brightness

For the reference brightness, the photography was performed with the settings of the reference shown in Table 3. The results in $65,536$

Table 5
Mean relative error and maximum relative error of $E_{e,n}/E_{e,n+k}$ with respect to B-, G-, and R-channels, and the focal length $f = 18$ mm, 35 mm, and 55 mm.

Focal length f (mm)	Mean relative error % (Maximum error %)		
	Color		
	B	G	R
18	9.57 (34.34)	9.56 (33.46)	9.61 (33.98)
35	7.81 (30.65)	7.29 (28.88)	7.75 (28.98)
55	7.20 (29.03)	6.82 (29.26)	7.13 (29.31)

(16-bit) levels for B-, G-, and R-channels are as follows: $V_B = 16874.3$, $V_G = 17755.1$, and $V_R = 8017.8$, respectively. We define the results above as the reference brightness, V_{ref}, (i.e., $V_{ref,B}$, $V_{ref,G}$, and $V_{ref,R}$).

4.5.2. V–k relation

Fig. 18 (top panel) indicate the pixel values $V_{II,B}$, $V_{II,G}$, and $V_{II,R}$ vs. the F-number difference k. For $r = 1$ (i.e., $\Phi_e = \Phi_{e,ref}$), and $r = 1/2$ (i.e., $\Phi_e = (1/2)\Phi_{e,ref}$), the pixel values $V_{II,B}$, $V_{II,G}$, and $V_{II,R}$ decrease with increasing the F-number difference k. From Eq. (15), the pixel value V'_I (brightness) to the reference (V_{ref}) is expressed by

$$V'_I = rV_I = V_{II} 2^k \frac{G_{ref}}{G_{II}} \frac{t_{ref}}{t_{II}} \frac{\beta_{ref}}{\beta_{II}} \frac{S_{ref}}{S_{II}} \frac{C_{FD,II}}{G_{FD,ref}} = V_{II} 2^k, \tag{31}$$

where G_{ref}/G_{II}, t_{ref}/t_{II}, β_{ref}/β_{II}, S_{ref}/S_{II}, and $C_{FD,II}/C_{FD,ref}$ vanish, as the settings of "Reference Photo" and "Photo II" except for the F-number were the same, i.e., $G_{II} = G_{ref}$ and $t_{II} = t_{ref}$, and the single camera explained in
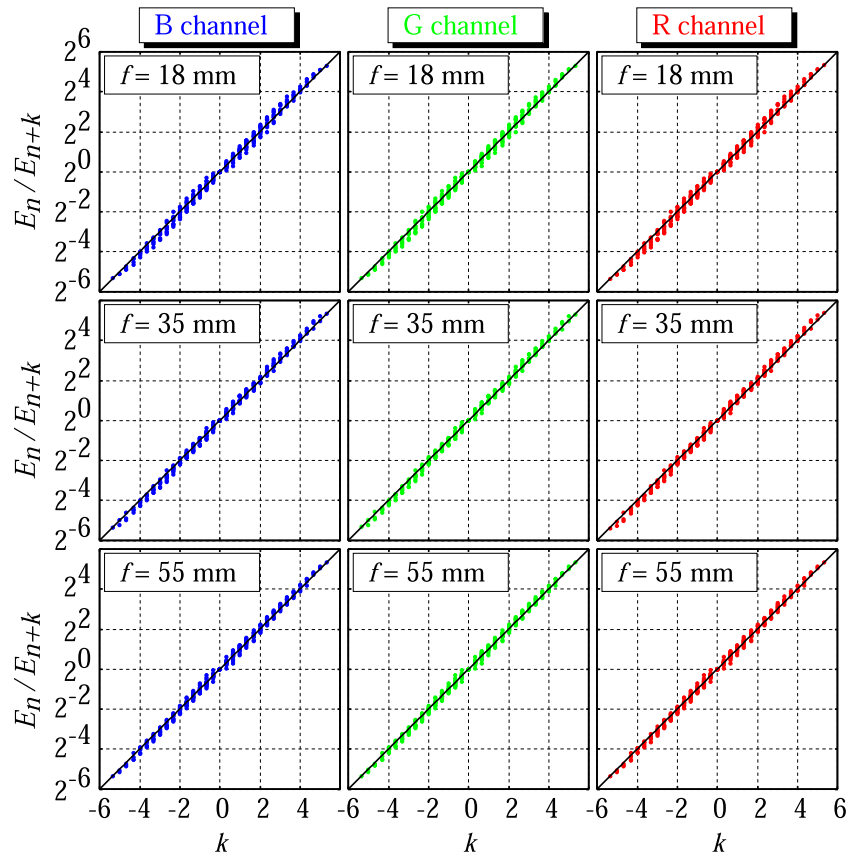

Fig. 17. Irradiance ratio $E_{e,n}/E_{e,n+k}$ vs. F-number difference k with respect to the B-, G-, and R-channels, the focal length (Top panel) $f = 18$ mm, (Middle panel) 35 mm, and (Bottom panel) 55 mm, and the ISO gain $G = 100$. The solid curves are the theoretical curve (2^k).
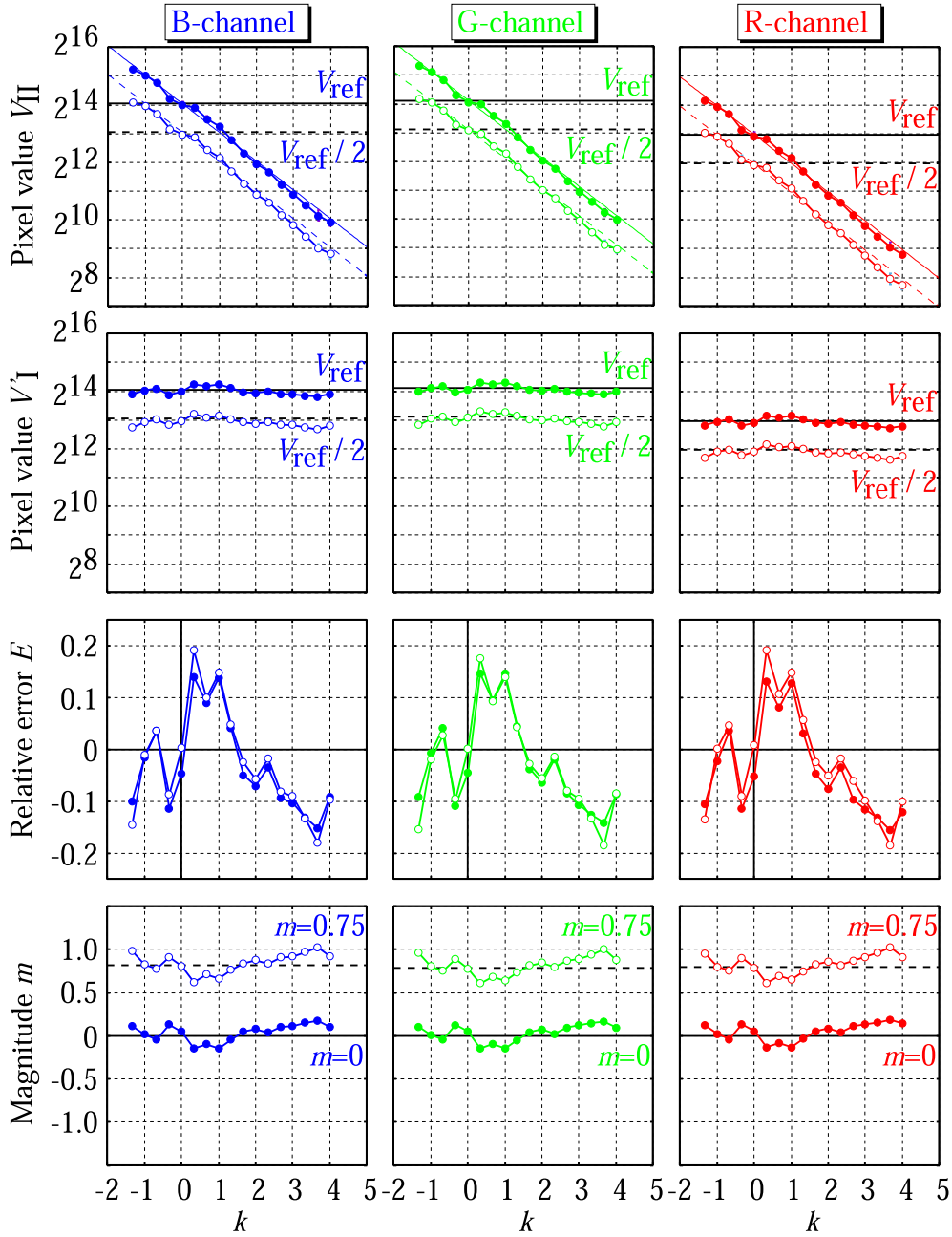
Fig. 18. (Top panel) Pixel values $V_{\mathrm{II,B}}$, $V_{\mathrm{II,G}}$, and $V_{\mathrm{II,R}}$ vs. the F-number difference k, (Second panel) pixel values $V'_{\mathrm{I,B}}$, $V'_{\mathrm{I,G}}$, and $V'_{\mathrm{I,R}}$ vs. k, (Third panel) these relative errors $E_{\mathrm{B}}, E_{\mathrm{G}}$, and E_{R} vs. k, and (Bottom panel) these magnitudes $m_{\mathrm{B}}, m_{\mathrm{G}}$, and m_{R} vs. k. The thick solid and dashed horizontal lines in (Top panel) and (Second panel) indicate the pixel values V_{ref}, of the reference (i.e., $r = 1$), and $V_{\mathrm{ref}}/2$, (i.e., $r = 1/2$), respectively (see §4.5.1). The thin solid line and thin dashed line in (Top panel) indicate the theoretical curves $V_{\mathrm{ref}}/2^k$ for $r = 1$, and $(1/2)V_{\mathrm{ref}}/2^k$ for $r = 1/2$, respectively (see Eq. (32)).

§3.1 was used, i.e., $\beta_{\mathrm{II}} = \beta_{\mathrm{ref}}$, $S_{\mathrm{II}} = S_{\mathrm{ref}}$, and $C_{\mathrm{FD,II}} = C_{\mathrm{FD,ref}}$. Therefore, the theoretical curve of V_{II} is expressed by

$$V_{\mathrm{II}} = \frac{1}{2^k} r\, V_{\mathrm{I}} = \frac{1}{2^k} r\, V_{\mathrm{ref}}, \tag{32}$$

where V_{I} is fixed to V_{ref}. Eq. (32) is shown in Fig. 18 (top panel) (thin solid line for $r = 1$ and thin dashed line for $r = 1/2$) with the pixel value V_{II} by experiment.

Fig. 18 (second panel) show the pixel values $V'_{\mathrm{I,B}}$, $V'_{\mathrm{I,G}}$, and $V'_{\mathrm{I,R}}$ vs. k. In Fig. 18 (second panel), the pixel values $V'_{\mathrm{I,B}}$, $V'_{\mathrm{I,G}}$, and $V'_{\mathrm{I,R}}$ (i.e., Eq. (31)) for $r = 1$ are distributed near $V_{\mathrm{ref,B}}$, $V_{\mathrm{ref,G}}$, and $V_{\mathrm{ref,R}}$, respectively. Similarly, $V'_{\mathrm{I,B}}$, $V'_{\mathrm{I,G}}$, and $V'_{\mathrm{I,R}}$ for $r = 1/2$ are distributed near $V_{\mathrm{ref,B}}/2$,

$V_{\mathrm{ref,G}}/2$, and $V_{\mathrm{ref,R}}/2$, respectively. We can see the pixel values $V'_{\mathrm{I,B}}$, $V'_{\mathrm{I,G}}$, and $V'_{\mathrm{I,R}}$ have errors (see Fig. 18 (second panel)).

Fig. 18 (third panel) indicate the relative errors $E_{\mathrm{B}}, E_{\mathrm{G}}$, and E_{R} for $V'_{\mathrm{I,B}}$, $V'_{\mathrm{I,G}}$, and $V'_{\mathrm{I,R}}$ in Fig. 18 (second panel), i.e., $E = (V'_{\mathrm{I}} - V_{\mathrm{ref}})/V_{\mathrm{ref}}$. These errors can be regarded as the error $(1 + \delta_{\mathrm{Lens}})(1 + \delta_{\mathrm{Sensor}})$, which is explained in §2.4 and Eq. (19). As the pixel value is the average of 10 experiments, the error of the image sensor is reduced, i.e., $(1 + \delta_{\mathrm{Lens}})(1 + \delta_{\mathrm{Sensor}}) \simeq (1 + \delta_{\mathrm{Lens}})$. That is, the error shown in Fig. 18 (third panel) are the intrinsic error $(1 + \delta_{\mathrm{Lens}})$ of the zoom lens. Dividing V'_{I} in Fig. 18 (second panel) by $(1 + \delta_{\mathrm{Lens}})$ results in V_{ref}. Therefore, accurate photometry will be possible if the intrinsic error $(1 + \delta_{\mathrm{Lens}})$ of the zoom lens can be obtained in advance before performing photometry.
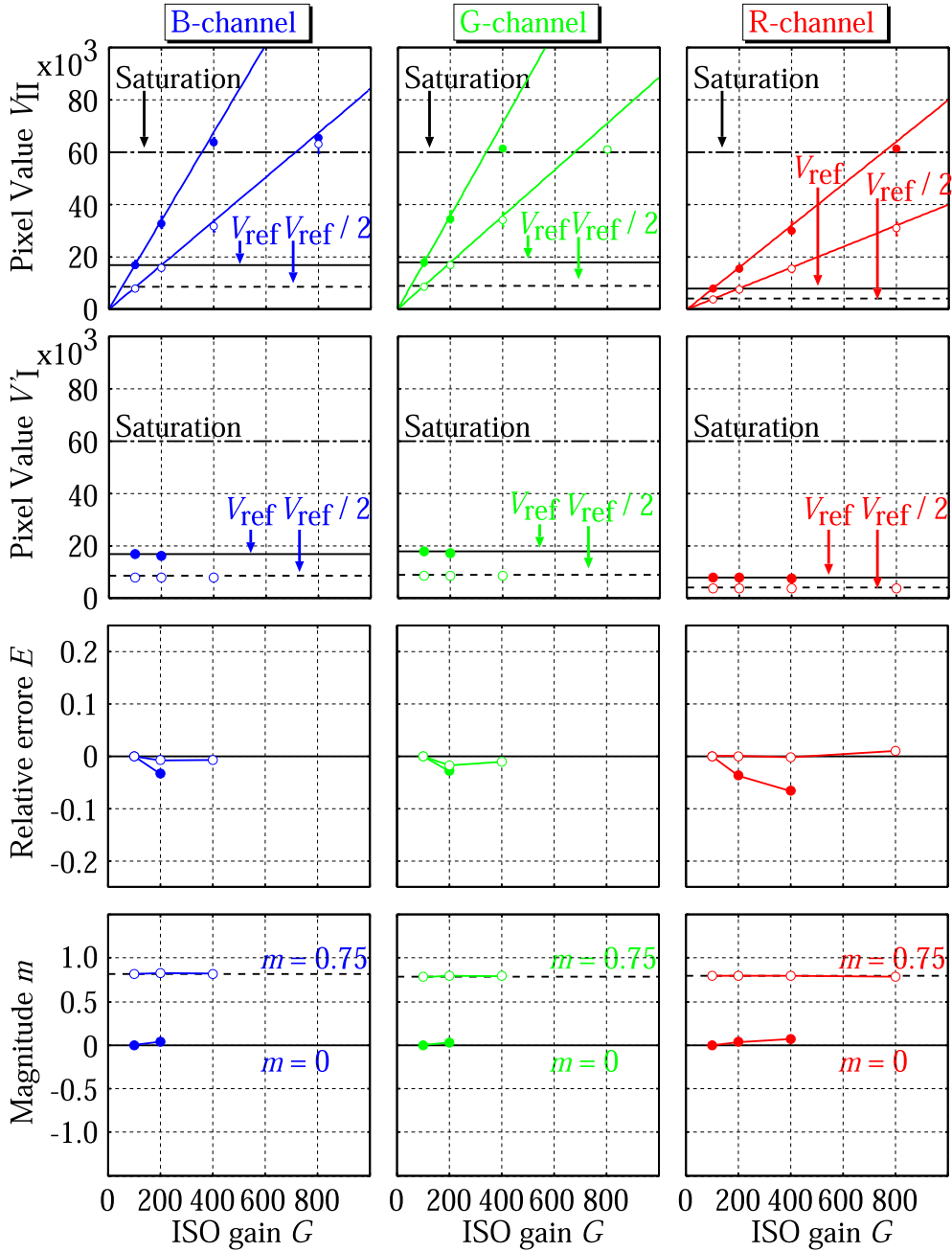
Fig. 19. (Top panel) Pixel value V_{II} vs. the ISO gain G, (Second panel) pixel value V'_I vs. the ISO gain G, (Third panel) these relative errors E vs. the ISO gain G, and (Bottom panel) these magnitude m vs. the ISO gain G. The thick solid and dashed horizontal lines in (Top panel) and (Second panel) indicate the pixel values V_{ref}, of the reference (i.e., $r = 1$), and $V_{ref}/2$, (i.e., $r = 1/2$), respectively (see §4.5.1). The thick dotted-dashed horizontal lines in (Top panel) and (Second panel) indicate the saturation line. The thin solid line and thin dashed line in (Top panel) indicate the theoretical curves $V_{ref} n$ for $r = 1$, and $(1/2)V_{ref} n$ for $r = 1/2$, respectively (see Eq. (36)).

Fig. 18 (bottom panel) indicate the magnitudes m_B, m_G, and m_R for $V'_{I,B}$, $V'_{I,G}$, and $V'_{I,R}$ in Fig. 18 (second panel). From Eq. (31), the magnitude m is given by

$$m = -2.5\log_{10}\frac{V'_I}{V_{ref}} = -2.5\log_{10}\frac{V_{II}}{V_{ref}}2^k, \tag{33}$$

where $r = 1$ or $r = 1/2$ herein. Ideally, the magnitudes m_B, m_G, and m_R should be distributed near $m = 0$ for $r = 1$, and $m = 0.75$ ($\simeq -2.5\log_{10}0.5$) for $r = 1/2$. However, these magnitudes (Fig. 18 (bottom panel)) have errors due to the intrinsic errors $(1 + \delta_{Lens,B})$, $(1 + \delta_{Lens,G})$, and $(1 + \delta_{Lens,R})$ in Fig. 18 (third panel). The accurate magnitude m (i.e., $m = 0$ for $r = 1$ and $m = 0.75$

for $r = 1/2$) will be obtained, if the correction of the intrinsic error $(1 + \delta_{Lens})$ of the zoom lens (Fig. 18 (third panel)) is performed.

4.5.3. V–G relation

Fig. 19 (top panel) indicate the pixel values $V_{II,B}, V_{II,G}, V_{II,R}$ vs. the ISO gain G. For $r = 1$ (i.e., $\Phi_e = \Phi_{e,ref}$), the pixel values $V_{II,B}$ and $V_{II,G}$ saturate at ISO gain $G = 400$, and $V_{II,R}$ is at $G = 800$, and for $r = 1/2$ (i.e., $\Phi_e = (1/2)\Phi_{e,ref}$), the pixel values $V_{II,B}$ and $V_{II,G}$ saturate at $G = 800$, and $V_{II,R}$ is at $G = 1600$ (see Fig. 19 (top panel)). From Eq. (15), the pixel value (brightness) to the reference is given by
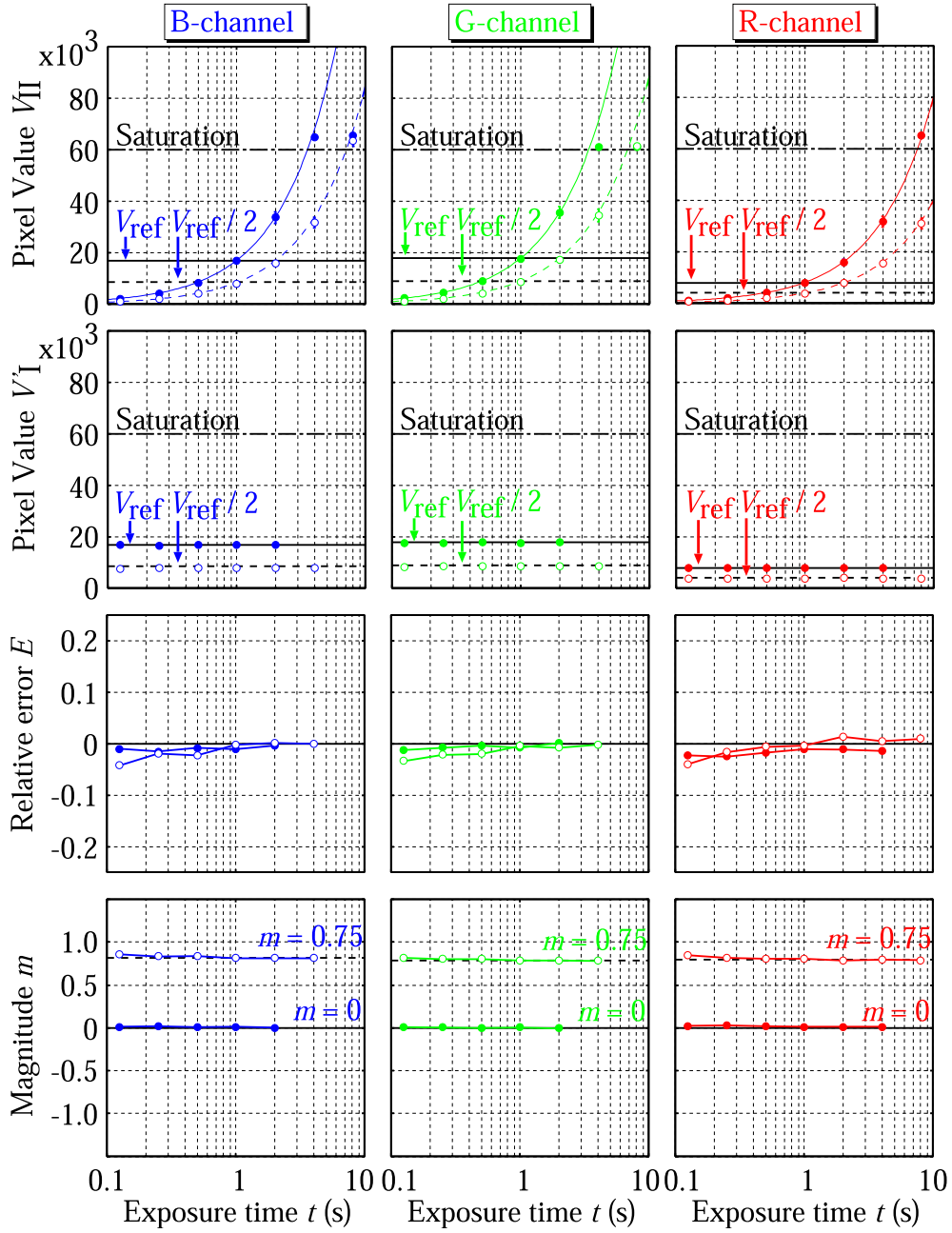
Fig. 20. (Top panel) Pixel values V_{II} vs. the exposure time t_{exp}, (Second panel) pixel values V'_{I} vs. the exposure time t_{exp}, (Third panel) these relative errors E vs. t_{exp}, and (Bottom panel) these magnitudes m vs. t_{exp}. The thick solid and dashed horizontal lines in (Top panel) and (Second panel) indicate the pixel values V_{ref}, of the reference (i.e., $r = 1$), and $V_{\mathrm{ref}}/2$, (i.e., $r = 1/2$), respectively (see §4.5.1). The thick dotted-dashed horizontal lines in (Top panel) and (Second panel) indicate the saturation line. The thin solid line and thin dashed line in (Top panel) indicate the theoretical curves $V_{\mathrm{ref}} t_{\mathrm{exp}}$ for $r = 1$, and $(1/2)V_{\mathrm{ref}} t_{\mathrm{exp}}$ for $r = 1/2$, respectively (see Eq. (40)).

$$V'_{\mathrm{I}} = rV_{\mathrm{I}} = V_{\mathrm{II}}\, 2^k\, \frac{G_{\mathrm{ref}}}{G_{\mathrm{II}}} \frac{t_{\mathrm{ref}}}{t_{\mathrm{II}}} \frac{\beta_{\mathrm{ref}}}{\beta_{\mathrm{II}}} \frac{S_{\mathrm{ref}}}{S_{\mathrm{II}}} \frac{C_{\mathrm{FD,II}}}{C_{\mathrm{FD,ref}}} \tag{34}$$

$$= V_{\mathrm{II}}\frac{G_{\mathrm{ref}}}{G_{\mathrm{II}}} = V_{\mathrm{II}}\frac{G_{\mathrm{ref}}}{n \times G_{\mathrm{ref}}} = V_{\mathrm{II}}\frac{1}{n}, \tag{35}$$

where $k = 0$, $G_{\mathrm{II}} = n \times G_{\mathrm{ref}}$, and the ratios $t_{\mathrm{ref}}/t_{\mathrm{II}}$, $\beta_{\mathrm{ref}}/\beta_{\mathrm{II}}$, $S_{\mathrm{ref}}/S_{\mathrm{II}}$, and $C_{\mathrm{FD,II}}/C_{\mathrm{FD,ref}}$ vanish, as the numerator and denominator of each ratio are the same. Therefore, the theoretical curve (solid lines in Fig. 19 (top panel)) is expressed as

$$V_{\mathrm{II}} = V_{\mathrm{I}}m = V_{\mathrm{ref}}m, \tag{36}$$

where V_{I} is fixed to V_{ref}. Eq. (36) means that the pixel values $V_{\mathrm{II,B}}, V_{\mathrm{II,G}}$, and $V_{\mathrm{II,R}}$ increase n times with the ISO gain G is increasing n times.

Fig. 19 (second panel) are the pixel values $V'_{\mathrm{I,B}}, V'_{\mathrm{I,G}}$, and $V'_{\mathrm{I,R}}$ vs. the ISO gain G. The plots in Fig. 19 (second panel) are the pixel values obtained by Eq. (35). The pixel values $V'_{\mathrm{I,B}}, V'_{\mathrm{I,G}}$, and $V'_{\mathrm{I,R}}$ for $r = 1$ and the unsaturation (i.e., $V_{\mathrm{II,B}}, V_{\mathrm{II,G}}, V_{\mathrm{II,R}} \leqslant 60,000$ in $65,536$ levels) are distributing near the references $V_{\mathrm{ref,B}}, V_{\mathrm{ref,G}}$, and $V_{\mathrm{ref,R}}$. The pixel values $V'_{\mathrm{I,B}}, V'_{\mathrm{I,G}}$, and $V'_{\mathrm{I,R}}$ for $r = 1/2$ and the unsaturation are distributed near $V_{\mathrm{ref,B}}/2, V_{\mathrm{ref,G}}/2$, and $V_{\mathrm{ref,R}}/2$. The pixel values $V'_{\mathrm{I,B}}, V'_{\mathrm{I,G}}$, and $V'_{\mathrm{I,R}}$ in Fig. 19 (second panel) have errors.

Fig. 19 (third panel) indicate the relative errors $E_{\mathrm{B}}, E_{\mathrm{G}}$, and E_{R} for $V'_{\mathrm{I,B}}, V'_{\mathrm{I,G}}$, and $V'_{\mathrm{I,R}}$ in Fig. 19 (second panel). These errors are due to the error δ_{Sensor} of the image sensor in the digital camera used herein (also see §2.4 and Eq. (19)). With respect to the unsaturated pixel, the errors

12

$\delta_{\text{Sensor,B}}$, $\delta_{\text{Sensor,G}}$, and $\delta_{\text{Sensor,R}}$ for the respective B-, G-, and R-channels are in the range $\sim \pm 5\%$. By increasing the number of experimental trials (photography), the error of the image sensor can be suppressed.

Fig. 19 (bottom panel) indicate the magnitudes m_{B}, m_{G}, and m_{R} for $V'_{\text{I,B}}$, $V'_{\text{I,G}}$, and $V'_{\text{I,R}}$ in Fig. 19 (second panel). The magnitude is given by

$$m = -2.5\log_{10}\frac{V'_{\text{I}}}{V_{\text{ref}}} = -2.5\log_{10}\frac{V_{\text{II}}}{V_{\text{ref}}}\frac{1}{n}, \tag{37}$$

where we used Eq. (35). The absolute errors of the magnitude m with respect to B-, G-, and R-channels are less than approximately 0.05 for the unsaturated pixel.

4.5.4. V–t_{exp} relation

Fig. 20 (top panel) indicate the pixel values $V_{\text{II,B}}$, $V_{\text{II,G}}$, and $V_{\text{II,R}}$ vs. the exposure time t_{exp}. For $r = 1$ (i.e., $\Phi_{\text{e}} = \Phi_{\text{e,ref}}$), the pixel values $V_{\text{II,B}}$, $V_{\text{II,G}}$, saturate at $t_{\text{exp}} = 4$ s, and $V_{\text{II,R}}$ is at $t_{\text{exp}} = 8$ s, and for $r = 1/2$ (i.e., $\Phi_{\text{e}} = (1/2)\Phi_{\text{e,ref}}$), the pixel values $V_{\text{II,B}}$, $V_{\text{II,G}}$, saturate at $t_{\text{exp}} = 8$ s, and $V_{\text{II,R}}$ is at $t_{\text{exp}} = 16$ s. From Eq. (15), the pixel value (brightness) to the reference is given by

$$V'_{\text{I}} = rV_{\text{I}} = V_{\text{II}}2^k\frac{G_{\text{ref}}}{G_{\text{II}}}\frac{t_{\text{ref}}}{t_{\text{II}}}\frac{\beta_{\text{ref}}}{\beta_{\text{II}}}\frac{S_{\text{ref}}}{S_{\text{II}}}\frac{C_{\text{FD,II}}}{C_{\text{FD,ref}}} \tag{38}$$

$$= V_{\text{II}}\frac{t_{\text{ref}}}{t_{\text{II}}} = V_{\text{II}}\frac{t_{\text{ref}}}{t \times t_{\text{ref}}} = V_{\text{II}}\frac{1}{t}, \tag{39}$$

where $k = 0, t_{\text{ref}} = 1$ s, $t_{\text{II}} = t \times t_{\text{ref}}$, and the ratios $G_{\text{ref}}/G_{\text{II}}$, $\beta_{\text{ref}}/\beta_{\text{II}}$, $S_{\text{ref}}/S_{\text{II}}$, and $C_{\text{FD,II}}/C_{\text{FD,ref}}$ vanish, as the numerator and denominator of each ratio are the same. Therefore, the theoretical curve (solid curves in Fig. 20 (top panel)) is expressed as

$$V_{\text{II}} = V_{\text{I}}rt = V_{\text{ref}}rt, \tag{40}$$

where V_{I} is fixed to V_{ref}. Eq. (40) indicates that the pixel values $V_{\text{II,B}}$, $V_{\text{II,G}}$, and $V_{\text{II,R}}$ increase t times with the exposure time t_{exp} is increasing t times.

Fig. 20 (second panel) are the pixel values $V'_{\text{I,B}}$, $V'_{\text{I,G}}$, and $V'_{\text{I,R}}$ vs. the exposure time t_{exp}. The plots in Fig. 20 (second panel) are the pixel values obtained by Eq. (39). The pixel values $V'_{\text{I,B}}$, $V'_{\text{I,G}}$, and $V'_{\text{I,R}}$ in Fig. 20 (second panel) for $r = 1$ and the unsaturation (i.e., $V_{\text{II,B}}$, $V_{\text{II,G}}$, $V_{\text{II,R}}$ $\leqslant 60,000$ in $65,536$ levels) are distributed near $V_{\text{ref,B}}$, $V_{\text{ref,G}}$, and $V_{\text{ref,R}}$. Similarly, the pixel values $V'_{\text{I,B}}$, $V'_{\text{I,G}}$, and $V'_{\text{I,R}}$ for $r = 1/2$ are distributed near $V_{\text{ref,B}}/2$, $V_{\text{ref,G}}/2$, and $V_{\text{ref,R}}/2$. The pixel values $V'_{\text{I,B}}$, $V'_{\text{I,G}}$, and $V'_{\text{I,R}}$ have errors.

Fig. 20 (third panel) indicate the relative errors E_{B}, E_{G}, and E_{R} for $V'_{\text{I,B}}$, $V'_{\text{I,G}}$, and $V'_{\text{I,R}}$ in Fig. 20 (second panel). With respect to the unsaturated pixel, the relative errors E_{B}, E_{G}, and E_{R} are in the range about $\pm 5\%$. These errors are due to not an intrinsic error of the zoom lens but the thermal noise on the image sensor of the used digital camera. Thus, these relative errors are regarded as the error δ_{Sensor} of the image sensor (also see §2.4 and Eq. (19)). Thus, these errors can be suppressed by increasing the number of experimental trials (photography). If possible, cooling can reduce the error δ_{Sensor} by thermal noise (see Ref. Budding and Demircan (2007) §6.3.1).

Fig. 20 (bottom panel) indicate the magnitudes m_{B}, m_{G}, and m_{R} for $V'_{\text{I,B}}$, $V'_{\text{I,G}}$, and $V'_{\text{I,R}}$ in Fig. 20 (second panel). The magnitude is given by

$$m = -2.5\log_{10}\frac{V'_{\text{I}}}{V_{\text{ref}}} = -2.5\log_{10}\frac{V_{\text{II}}}{V_{\text{ref}}}\frac{1}{t}, \tag{41}$$

where we used Eq. (39). The absolute errors of the magnitude m with respect to B-, G-, and R-channels are less than approximately 0.1 for the unsaturated pixel. These are sufficiently small; furthermore, by increasing the number of experimental trials (photography) and by cooling the image sensor, the error of the magnitudes m_{B}, m_{G}, and m_{R} can be suppressed.

5. Conclusions

The results of the image sensor properties showed that the pixel value V is linear with errors ($< \sim 5\%$) in the range less than the satu-

ration value. The results of the lens properties suggested that the pixel value V depends on the focal length, although the F-number is constant. This is due to the intrinsic error of the zoom lens. The results of the lens properties also showed that the irradiance ratio $E_{\text{e},n}/E_{\text{e},n+k}$ is distributed near the curve 2^k, although the effect of the intrinsic error of the zoom lens is included. The intrinsic error δ_{Lens} of the zoom lens can be correct by dividing the pixel value V by $(1 + \delta_{\text{Lens}})$. Thus, the equation $E_{\text{e},n}/E_{\text{e},n+k} = 2^k$ can be used in photometry.

In photometry, the maximum intrinsic error of the zoom lens was about 20%, and the error of the image sensor obtained for the exposure time and the ISO gain is less than $\sim 5\%$. As the intrinsic error of the zoom lens is not a random noise, it can be corrected. The error of the image sensor can be reduced by increasing the number of experimental trials. The absolute error of the magnitude was less than 0.05, and thus it is applicable to general photometry.

6. Summary

We formulated the pixel value (i.e., brightness) to a reference and proporsed using the magnitude system, which was developed in astronomical photometry, for widespread general photometry. The results of photometry performed herein with the single camera suggested that the formula of the pixel value to the reference, and the magnitude system can be applicable to photometry. The intrinsic error of the zoom lens was observed to be correct.

7. Future work

In this study, the photometry using the single camera was performed. In future, photometry using different cameras needs to be performed, and to verify the correctness of the formula of the pixel value to the reference using different cameras, which was derived in this work. It also needs to consider using the reference star, such as Vega in astronomy, as the standard reference light source, or developing the standard reference light source.

Declaration of Competing Interest

The authors declare that they have no known competing financial interests or personal relationships that could have appeared to influence the work reported in this paper.

Appendix A. Photography kit

To evaluate an image sensor in a digital camera and the optical properties of the zoom lens, a tabletop darkroom (see Fig. 6) was developed by improving a PC rack. To shield ambient light, the left and right sides and back of the PC rack were covered by black cloth

(cotton 100%), and its front side was by the black cloth (felt). Suppressing the light reflection inside the darkroom, the top shelf of the PC rack and four vertical mounting columns supporting the top shelf were covered by the black cloth (cotton 100%), and an optical breadboard colored black (THORLABS, ALUMINIUM BREADBOARD, MB6060/M, $600 \times 600 \times 12.7$ mm) was on the tabletop of the PC rack.

A light source, which is a constant-current driven white-LED light source, was developed (see Fig. 7). The power supply of the light source was used Ni-MH rechargeable batterys (06P, 8.4 V), since an AC-DC converter generates noise. As the voltage of a battery, in general, slightly changes below with long time use, the luminance of the LED will change. Thus, the white-LED of the light source was driven by the constant-current circuit (Fig. 7).

The photosensor was driven by the dual-tracking power supply comprising two Ni-MH rechargeable batteries for the same reason explained above. As the photocurrent generated by the photodiode PD is extremery small, I–V conversion was performed by the transimpedance amplifier shown in Fig. 8.

The circuit boards of the LED light source and photosensor were made for processing with the milling machine (FP-21T, MITS Electronics).

References

Hönel, A., Posch, T., Ribas, S.J., Aubé, M., Duriscoe, D., Jechow, A., Kollath, Z., Lolkema, D.E., Moore, C., Schmidt, N., Spoelstra, H., Wuchterl, G., Kyba, C.C., 2018. Measuring night sky brightness: methods and challenges. J. Quant. Spectrosc. Radiat. Transf. 205, 278–290. https://doi.org/10.1016/j.jqsrt.2017.09.008.

Jechow, A., Ribas, S.J., Domingo, R.C., Hölker, F., Kolláth, Z., Kyba, C.C., 2018. Tracking the dynamics of skyglow with differential photometry using a digital camera with fisheye lens. J. Quant. Spectrosc. Radiat. Transf. 209, 212–223. https://doi.org/10.1016/j.jqsrt.2018.01.032.

Jechow, A., Kyba, C.C., Hölker, F., 2020. Mapping the brightness and color of urban to rural skyglow with all-sky photometry. J. Quant. Spectrosc. Radiat. Transf. 250. https://doi.org/10.1016/j.jqsrt.2020.106988. 106988.

Kolláth, Z., Cool, A., Jechow, A., Kolláth, K., Száz, D., Tong, K.P., 2020. Introducing the dark sky unit for multi-spectral measurement of the night sky quality with commercial digital cameras. J. Quant. Spectrosc. Radiat. Transf. 253. https://doi.org/10.1016/j.jqsrt.2020.107162. 107162.

Syrjäsuo, M.T., Donovan, E.F., 2004. Diurnal auroral occurrence statistics obtained via machine vision. Ann. Geophys. 22, 1103–1113.

Flowers, J.W., 1943. The channel of the spark discharge. Phys. Rev. 64, 225–235. https://doi.org/10.1103/PhysRev.64.225.

Idone, V.P., Orville, R.E., 1985. Correlated peak relative light intensity and peak current in triggered lightning subsequent return strokes. J. Geophys. Res. 90, 6159–6164. https://doi.org/10.1029/JD090iD04p06159.

Gomes, C., Cooray, V., 1998. Correlation between the optical signatures and current wave forms of long sparks: applications in lightning research. J. Electrostat. 43, 267–274. https://doi.org/10.1016/S0304-3886(98)00008-4.

Wang, D., Takagi, N., Watanabe, T., Rakov, V.A., Uman, M.A., Rambo, K.J., Stapleton, M.V., 2005. A comparison of channel-base currents and optical signals for rocket-triggered lightning strokes. Atmos. Res. 76, 412–422. https://doi.org/10.1016/j.atmosres.2004.11.025.

Amarasinghe, D., Sonnadara, U., Berg, M., Cooray, V., 2007. Correlation between brightness and channel currents of electrical discharges. IEEE Trans. Diel. Electr. Insul. 14, 1154–1160. https://doi.org/10.1109/TDEI.2007.4339475.

Zhou, E., Lu, W., Zhang, Y., Zhu, B., Zheng, D., Zhang, Y., 2013. Correlation analysis between the channel current and luminosity of initial continuous and continuing current processes in an artificially triggered lightning flash. Atmos. Res. 129–130, 79–89. https://doi.org/10.1016/j.atmosres.2012.10.020.

Shimoji, N., Aoyama, R., Hasegawa, W., 2016. Spatial variability of correlated color temperature of lightning channels. Results Phys. 6, 161–162. https://doi.org/10.1016/j.rinp.2016.03.004.

Shimoji, N., Kuninaka, S., Izumi, K., 2017. Evaluation of the brightness of lightning channels and branches using the magnitude system: application of astromonical photometry. Results Phys. 7, 2085–2095. https://doi.org/10.1016/j.rinp.2017.06.013.

Shimoji, N., Uehara, Y., 2017. Color analysis of lightning leaders: application of astronomical photometry. AIP Conf. Proc. 1906. https://doi.org/10.1063/1.5012310. 030030.

Shimoji, N., Nakano, T., 2019. Color analysis based on the color indices of lightning channels obtained from a digital photograph. Results Phys. 15,. https://doi.org/10.1016/j.rinp.2019.102662 102662.

Hecht, E., 2002. Optics, International Edition. Addison Wesley, USA.

Bigasa, M., Cabrujaa, E., Forestb, J., Salvib, J., 2006. Review of CMOS image sensors. Microelectron. J. 37, 433–451. https://doi.org/10.1016/j.mejo.2005.07.002.

Fossum, E.R., Hondongwa, D.B., 2014. A review of the pinned photodiode for CCD and CMOS image sensors. IEEE J. Electron Devices Soc. 2, 33–43. https://doi.org/10.1109/JEDS.2014.2306412.

Kusuhara, F., Wakashima, S., Nasuno, S., Kuroda, R., Sugawa, S., 2016. Analysis and reduction technologies of floating diffusion capacitance in CMOS image sensor for photon-countable sensitivity. ITE Trans. MTA 4, 91–98. https://doi.org/10.3169/mta.4.91.

Budding, E., Demircan, O., 2007. Introduction to Astronomical Photometry. Cambridge University Press, New York, US.